THE UNIVERSITY of TENNESSEE at CHATTANOOGA
COLLEGE of ENGINEERING and COMPUTER SCIENCE

SIMCENTER
NATIONAL CENTER for COMPUTATIONAL ENGINEERING

Channel Shape Design of Solid Oxide Fuel Cells

A Technical Report by

Sagar Kapadia
W. Kyle Anderson
and
Chad Burdyshaw

UTC-CECS-SimCenter-2009-01
June 2009

GRADUATE SCHOOL OF COMPUTATIONAL ENGINEERING
701 East M.L. King Boulevard • Chattanooga, TN 37403

CHANNEL SHAPE DESIGN OF SOLID OXIDE FUEL CELLS

S. Kapadia[1], W. K. Anderson[2], C. Burdyshaw[3]

University of Tennessee SimCenter at Chattanooga,
701, East M.L. King Boulevard, Chattanooga, TN – 37403, U.S.A.

Abstract

Shape optimization of fuel channels in solid oxide fuel cells (SOFC) is presented. A three-dimensional, implicit, multi-species fuel cell solver is developed to compute the baseline solution. Sensitivity derivatives required for the optimization are computed using the discrete adjoint method. A gradient based optimizer is utilized to update the design variables. The geometry of the fuel channel is parameterized to obtain meaningful design variables using a recently developed technique that is applicable for multi-disciplinary design optimization. During the design process, the mesh is continually modified to reflect the changes in the underlying geometry. An automated environment to sequentially execute the aforementioned processes is developed. Cost functions representating the cell voltage and uniform distribution of fuel among all channels are optimized with respect to the shape of the fuel channels.

Keywords: SOFC, fuel cell, shape, design, adjoint, sensitivity analysis

1. Introduction

Development of alternative energy producing devices has attracted a lot of attention from researchers all over the world in recent years. Due to its capability of producing

[1] Corresponding Author. Email: Sagar-Kapadia@utc.edu Tel: (001)4234255552 Fax: (001)4234255517
Present Address: University of Tennessee SimCenter at Chattanooga, TN-37403,U.S.A.
[2] Email: Kyle-Anderson@utc.edu
[3] Email: Chad-Burdyshaw@utc.edu

energy at higher efficiency and flexibility towards various hydrocarbon fuel types, Solid Oxide Fuel Cells (SOFCs) present a promising technology of the future. Even though SOFCs are still in the developmental stage, numerical techniques can be effectively utilized to find solutions to may of the design hurdles affecting the commercial application of the technology. Experimental and numerical approaches have been undertaken by several researchers [1-8] to study the behavior of SOFC. Some of the advantages of the numerical simulations over the experiments are the cost effectiveness and the fact that the simulations provide a wealth of data that is difficult or impossible to obtain experimentally and can be used to perform in-depth analysis of the SOFC unit/system. Numerical simulations can contribute greatly toward better designs that can produce more power, increased efficiency and extended life expectancy of various SOFC components.

To date, numerical simulations have been primarily focused on analysis of fuel cells or fuel cell components, without strong emphasis on utilizing the simulations in a design optimization environment. In particular, optimization procedures that may be efficiently used for a large number of design variables have not been developed. Because of the emphasis on analysis instead of design, sensitivity information to determine the effects of variations in design parameters on performance has been primarily implemented by simply changing the parameter of interest, re-running the simulation, and comparing the results with those from the original simulation [1,5-6,8]. While this approach can be used to determine the effects of parameter variations on fuel cell performance, a more rigorous approach toward optimization would likely lead to better designs, and can also provide improved insight into the parameters affecting the performance of the fuel cell. For SOFC

problems, example cost functions that can be used for improving performance include minimizing temperature variations, obtaining equal distribution of fuel in each of the channels, or maximizing power. Design variables may be related to the shape/size of the fuel channels, electrodes, electrolyte, and interconnect, but may also be coupled to the stoichiometric composition of fuel or material properties such as the porosity or tortuosity of the electrodes.

In references [9] and [10], optimization algorithms have been used to improve the performance of a polymer-electrolyte-membrane fuel cell (PEM) using four design variables, where the sensitivity derivatives used for the optimization algorithm have been obtained using a finite-difference approach. While finite differences are often a viable means for computing sensitivity derivatives, this method can be computationally restrictive when a sufficiently large number of design variables are present. In addition, accurate derivatives can sometimes be difficult to obtain using finite differences because of subtractive cancellation errors [11], which occur when the function evaluations in the numerator become computationally indistinguishable [12] when very small perturbations are used. By using a discrete adjoint method, sensitivity derivatives that are consistent with the flow solver may be obtained for use in a design optimization environment. A particular strength of adjoint methods is that sensitivity information can be obtained with a computational cost that is only weakly dependent on the number of design variables, and is therefore enabling technology for design studies where many design variables are required.

Secanell et al. [13] performed gradient-based optimization of a planar self-breathing polymer electrolyte membrane (PEM) fuel cell cathode using a two-dimensional

fuel cell model. Sensitivity derivatives of the current density were obtained using a direct-differentiation method with respect to the electrode design parameters. Although direct differentiation is an accurate method of obtaining sensitivity derivatives, application of this method for a practical design problem with many design variables is computationally expensive. Recently, Huang et al. [14] studied influence of flow uniformity in various interconnects on cell performance of SOFC. Even though shape optimization performed in the paper using Levenberg-Marquardt method (LMM) was interesting, sensitivity derivatives of the cost function with respect to each parameter were computed separately using finite difference method. This approach is not practical for design problems with a large number of parameters and finite difference method also suffers from subtractive cancellation errors. Similarly, channel design of proton exchange membrane fuel cell (PEMFC) performed by Lee et al. [15] lacked the inclusion of a technique to compute sensitivity derivatives. Lee et al. [15] utilized an approach to change the parameter of interest and study the effect on the final cost function. Even though such approach is useful, optimization performed with accurate sensitivity derivatives would be more efficient and effective, particularly when dealing with a complicated geometry and a large number of design variables.

In recent years, adjoint methods have been developed and utilized for numerical simulations in the aerodynamic community for sensitivity analysis, error estimation, and adaptive meshing [16-27]. Recently, Kapadia et al. [28] performed a sensitivity analysis for a three-dimensional fuel cell type geometry where the cost function was based on the requirement of equally distributing fluid through the channels. This numerical experiment

included all the mesh points defining the surface of the geometry as parameters, totaling more than 180,000 design variables. The adjoint method is particularly suited to this class of problem because the sensitivity derivatives can be obtained for all design variables with the computational cost of a single solution of the nonlinear system used for analysis, a single solution of the linear adjoint system, and a matrix-vector multiply. Although the numerical model used in this problem did not include diffusion or chemistry, it demonstrated the applicability of the adjoint method for solving problems with many design variables. To further demonstrate the use of the discrete adjoint method for SOFC applications, Kapadia et al. [28-30] implemented the adjoint method for one-dimensional [28], two-dimensional [29] and three-dimensional [30] SOFC models. In these studies, Kapadia et al. [26-28] computed sensitivity derivatives of several cost functions reflecting the performance of SOFC with respect to geometric and material properties of the fuel cell. In addition, an optimization of two-dimensional SOFC model [29] is performed that included material properties, operating conditions and fuel channel-anode assembly thickness as design parameters. One of the interesting cost functions optimized in this study was the standard deviation of the temperature inside that anode.

The primary goal of this paper is to formulate and develop adjoint methodology that accounts for high-fidelity physical modeling and can be applied to design various SOFC components in three-dimensions. Even though the methodology is general enough to address general shape design problems, this paper focuses on computing sensitivity derivatives of important cost functions with respect to shape of the fuel channel. Subsequently, sensitivity derivatives are used with a formal optimization method to modify

the shape of the fuel channels in order to improve the cost function. Two cases are demonstrated to emphasize the importance of shape optimization. The first case is a seventeen-channel manifold optimized to distribute the flow equally amongst all channels. This case does not include chemistry or electrochemistry, but demonstrates the capability of a design tool to tackle large scale problems. The second case represents a simplified geometry as compared to the first case, but includes complex physics present inside the fuel cell. The geometry for the second case can be termed as a single-channel SOFC, which includes fuel channel, air channel, anode, cathode, electrolyte and interconnects. The shape of the fuel channel is modified using the simulation tools to improve the cell voltage.

2. Governing Equations and Numerical Details

2.1 Governing Equations and Boundary Conditions

Case 1

As mentioned previously, two design problems have been included in this paper. The first problem deals with a complicated geometry but with simplified physics. The geometry is made up of a fuel cell manifold containing 17 fuel channels as shown in Figure 1(a) and (b). Geometrical dimensions are given in Table 1.

Inlet diameter	3.5 mm
Outlet diameter	3.5 mm
Channel length	46.0 mm
Channel width	2.0 mm
Channel height	1.5 mm
Distance between two consecutive channels	1.0 mm

Table 1. Geometrical dimensions of a manifold with 17 channels (Case 1)

This case does not include any other SOFC components (for example, anode, cathode etc.), chemistry or electrochemistry. The computational model, Figure 1(b), is based on an experimental geometry from the University of Arizona, Figure 1(a), but has been modified to only 17 fuel channels to reduce computational costs. The flowfield has been computed using an incompressible fluid assumption, with viscous flow in the laminar regime (Reynolds number is 182.0 based on inlet pipe diameter of 3.5 mm).

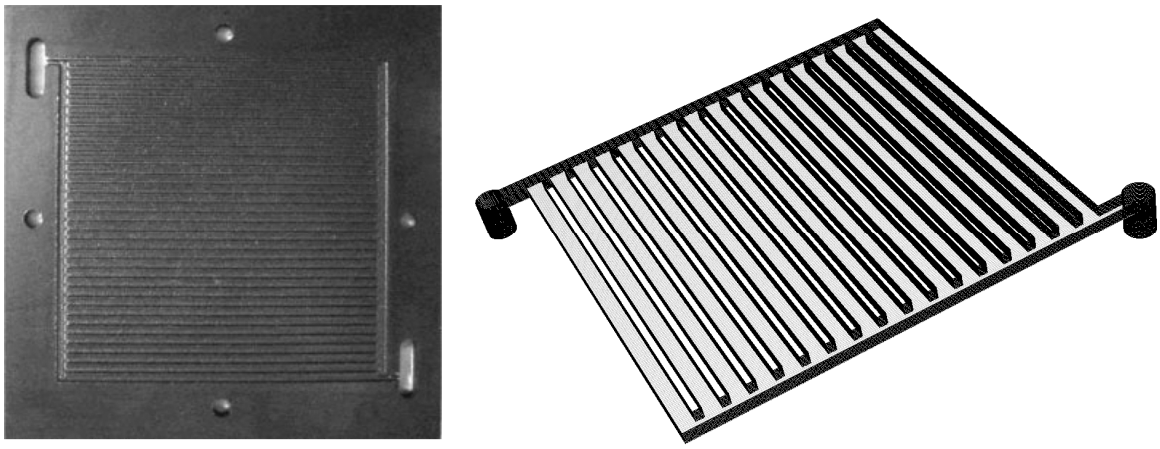

Figure 1(a) & (b). Experimental geometry and computational model (Case 1)

All solid walls present in the computational geometry, Figure 1(b) are treated as adiabatic walls and applied with no-slip boundary conditions. The mass flow rate is specified at the inlet of the manifold and back pressure is specified at the outlet of the manifold.

Case 2

The second design problem consists of a simplified geometry and more sophisticated physics including, multi-species diffusion, low-speed convection and chemical/electrochemical reactions. Various SOFC components including the anode, cathode, electrolyte, interconnects, the air and fuel channels are included in the geometry as shown in Figure 2. The figure shows the front view of the actual geometry used in the numerical simulation. Fuel and air channels are bored through the interconnects and a very thin electrolyte (0.05 mm) is sandwiched between the porous electrodes. Dimensions of the geometry are given in Table 2.

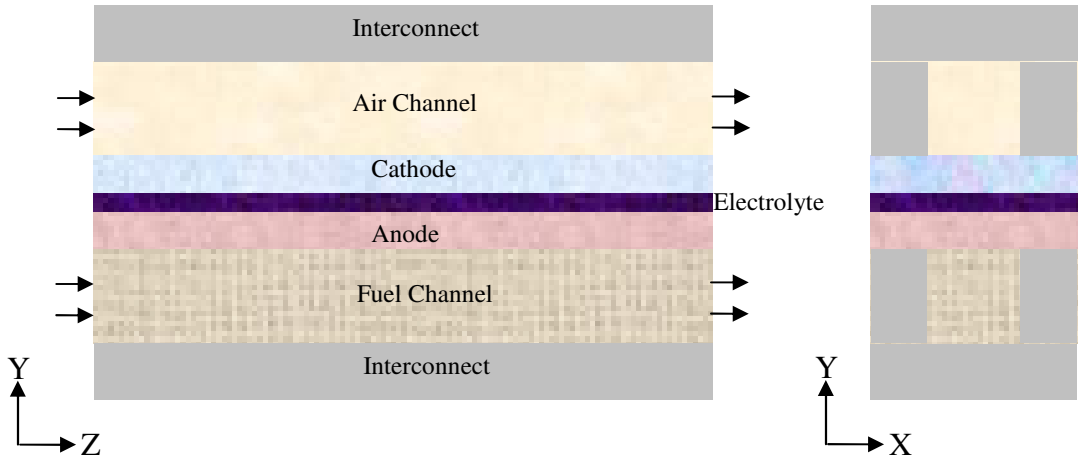

Figure 2(a) & (b). Computational model (Case2, side view and front view)

Length (z-direction)	40.0 mm
Width (x-direction)	9 mm
Height (y-direction)	16.925 mm
Anode thickness (y-direction)	0.625 mm
Cathode thickness (y-direction)	1.25 mm
Electrolyte thickness (y-direction)	0.05 mm
Channel width (x-direction)	5.0 mm
Channel thickness (y-direction)	5.0 mm

Table 2. Geometrical dimensions of planar type SOFC (Case 2)

Fuel and air enter through the inlet of the channels and diffuse inside the anode and cathode, respectively. Oxygen atoms combine with the electrons and get converted into oxygen ions ($0.5O_2 + 2e^- \rightarrow O^{2-}$). These oxygen ions migrate through the solid electrolyte to reach the anode-electrolyte interface and combine with hydrogen to generate steam and release electrons ($H_2 + O^{2-} \rightarrow H_2O + 2e^-$). Both these reactions take place inside extremely thin layers near the cathode-electrolyte and the anode-electrolyte interfaces, respectively. Because modeling the details of the interface region is impractical due to the small size, the cumulative effect of the electrochemical reactions is modeled as a jump in the electric potential, similar to the approach used by Ferguson et al.[1].

The three-dimensional SOFC model [30] utilized in this paper solves multi-species Navier-Stokes equations along with an electric potential equation that governs the distribution of electric potential and current density in the field. The three-dimensional model accounts for all components of the SOFC, including the anode, cathode, electrolyte, interconnects, and the fuel and air channels. Note that the model is not limited to any particular type of SOFC, i.e. planar as well as tubular type SOFC can be simulated using

this model. Results obtained using this model have previously been presented in [30] for a planar type porous-electrode supported SOFC as explained by Wang et al. [31].

Governing equations for the mass, momentum and energy conservation are solved simultaneously with the equation governing the electric potential in the numerical model. The system of equations utilized in the model is given by equations (1) - (6), which represent the conservation statements for the species concentrations, momentum (x, y and z), energy and current, respectively.

$$\frac{\partial(\varepsilon\rho_i)}{\partial t}+\nabla\bullet(\varepsilon\rho_i\vec{V})+\nabla\bullet(\vec{J_i})=S_i \tag{1}$$

$$\frac{\partial(\varepsilon\rho u)}{\partial t}+\nabla\bullet(\varepsilon\rho u\vec{V})=-\varepsilon\frac{\partial P}{\partial x}+\nabla\bullet(\varepsilon\tau_x)-\frac{\varepsilon^2 u\mu}{B} \tag{2}$$

$$\frac{\partial(\varepsilon\rho v)}{\partial t}+\nabla\bullet(\varepsilon\rho v\vec{V})=-\varepsilon\frac{\partial P}{\partial y}+\nabla\bullet(\varepsilon\tau_y)-\frac{\varepsilon^2 v\mu}{B} \tag{3}$$

$$\frac{\partial(\varepsilon\rho w)}{\partial t}+\nabla\bullet(\varepsilon\rho w\vec{V})=-\varepsilon\frac{\partial P}{\partial z}+\nabla\bullet(\varepsilon\tau_z)-\frac{\varepsilon^2 w\mu}{B} \tag{4}$$

$$\frac{\partial(\varepsilon E_t)}{\partial t}+\nabla\bullet(\varepsilon(E_t+P)\vec{V})+\nabla\bullet(\sum_{ns}\vec{J_i}H_i)=\nabla\bullet(\varepsilon\mu\tau\vec{V})-\nabla\bullet q^{eff}+\nabla\phi.(\sigma\nabla\phi) \tag{5}$$

$$\nabla\bullet(\sigma\nabla\phi)=0 \tag{6}$$

Equations (1) – (5) are modified Navier-Stokes equations valid for both porous and fluid regions. Detailed discussion on flux formulation for these equations can be found in previous work [26-28]. Equation (6) represents the electric potential equation. Electric/ionic conductivity, σ, in equation (6) is a strong function of the temperature. Expressions describing the relationships between the electric/ionic resistivity (reciprocal of conductivity) and the temperature for various components of SOFC are presented in Table

3 [31,32] along with thermal conductivities and other material properties of different components of the SOFC.

As presented, equation (6) is an elliptic equation contrary to the rest of the governing equations, equations (1) - (5), which are hyperbolic-parabolic equations. Equation (6) is solved in the entire domain except for the fuel and air channels, which are pure fluid regions. The lower boundary of the SOFC shown in Figure 2 (bottom surface of the interconnect) is assumed to be at zero potential while average current density is specified on the upper boundary of the interconnect at the top of the cell. Thus, the computed potential on the top surface of the interconnect gives the operating voltage of the SOFC. Similar boundary conditions have also been used in references [1, 6, 31].

Electric resistivity of anode $(\Omega - m)$	$2.98\times10^{-5}\exp(-1392/T)$
Electric resistivity of cathode $(\Omega - m)$	$8.11\times10^{-5}\exp(600/T)$
Electric resistivity of interconnect $(\Omega - m)$	6.41×10^{-8}
Ionic resistivity of electrolyte $(\Omega - m)$	$2.94\times10^{-5}\exp(10350/T)$
Thermal conductivity of anode $(W\,m_1K_1)$	6.23
Thermal conductivity of cathode $(W\,m_1K_1)$	9.6
Thermal conductivity of interconnect $(W\,m_1K_1)$	9.6
Thermal conductivity of electrolyte $(W\,m_1K_1)$	2.7
Porosity of anode	0.38
Porosity of cathode	0.5
Tortuosity of anode	1.5
Tortuosity of cathode	1.5
Permeability of anode $(m2)$	1.0×10^{-10}
Permeability of cathode $(m2)$	1.0×10^{-10}
Pore diameter of anode (m)	2.0×10^{-6}
Pore diameter of cathode (m)	2.0×10^{-6}

Table 3. Material properties of various components of SOFC [31, 32]

The voltage output of the SOFC strongly depends on several irreversibilities or losses encountered in the flowfield including activation polarization, concentration polarization and ohmic polarization. Noren and Hoffman [33] have provided extensive discussion on accurately modeling the activation polarization. The SOFC model used in this work employs the Butler-Volmer equation to compute activation polarization [33]. The Butler-Volmer equation can be written as,

$$i = i_0\left[\exp\left(\alpha\frac{n_e F}{R_u T}\eta_{act}\right) - \exp\left((1-\alpha)\frac{n_e F}{R_u T}\eta_{act}\right)\right] \tag{7}$$

The activation polarization is denoted by η_{act}.

α is the charge transfer coefficient and assumed to be 0.5 in the current work.

n_e represents the number of electrons involved in the electrochemical reaction, which is 2 in the current simulation.

i_0 is the exchange current density and it is computed using equations (8) and (9) for the anode and cathode [34], respectively.

$$i_{0,a} = \zeta_a \left(\frac{P_{H_2}}{P_{ref}} \right) \left(\frac{P_{H_2O}}{P_{ref}} \right) \exp\left(-\frac{E_{act,a}}{R_u T} \right) \tag{8}$$

$$i_{0,c} = \zeta_c \left(\frac{P_{O_2}}{P_{ref}} \right)^{0.25} \exp\left(-\frac{E_{act,c}}{R_u T} \right) \tag{9}$$

Various constants in the above equations are given in Table 4 [34]. Once the values of α and n_e are inserted in equation (7), the activation polarization can be computed using the following expression.

$$\eta_{act} = \left(\frac{R_u T}{F} \right) \sinh^{-1}\left(\frac{i}{2 i_0} \right) \tag{10}$$

α	0.5
n_e	2
$\zeta_a (A\ m_2)$	5.5×10^8
$\zeta_c (A\ m_2)$	7.0×10^8
$E_{act,a} (J\ kmol_1)$	1.0×10^8
$E_{act,c} (J\ kmol_1)$	1.2×10^8
$P_{ref} (N\ m_2)$	101325

Table 4. Constants used to compute activation polarization [34]

Ohmic polarization is a direct consequence of the resistance offered to the flow of electrons/ions inside various components of the SOFC. Voltage drop due to ohmic resistance is directly proportional to the current and the resistance. The effect of ohmic polarization on the voltage loss is directly included in the potential equation, equation (6), through the electric conductivity, σ, which is the reciprocal of the electric resistivity.

Concentration polarization is caused by reductions in the concentrations of the reacting species at the interface between the electrodes and the electrolyte. The effect of the reduction in concentrations can be seen from the well-known Nernst potential equation, given by equation (11). Also, exchange current densities at the anode-electrolyte interface and the cathode-electrolyte interface, represented by equations (8) and (9), respectively, are strongly affected by the concentration polarization.

Equation (11) computes the electromotive force (EMF) or electric potential under reversible conditions, i.e. in the absence of activation, ohmic or any other losses.

$$EMF = EMF^0 + \frac{RT}{2F}\ln\left(\frac{\overline{P}_{H_2}\overline{P}_{O_2}^{0.5}}{\overline{P}_{H_2O}}\right) \tag{11}$$

$$\overline{P}_i = \frac{P_i}{P_{ref}} \tag{12}$$

The electromotive force at standard pressure is given by EMF^0. The value of P_{ref} is taken as one atmosphere in above equation.

The electrochemical reaction reduces the concentration of the reactants and increases the concentration of the products at the electrode-electrolyte interface. Thus, the partial pressures of the reactants and products are affected in the same manner. This will

reduce the value of the second term on the right-hand side of the equation (11) thereby affecting the EMF of the cell adversely. Concentration polarization strongly depends on the material properties of the electrodes that are responsible for the transport (diffusion and convection) of the reactants and products, to and from the electrode-electrolyte interface.

No-slip, adiabatic wall boundary conditions are applied at the top wall, bottom wall and side walls of the computational geometry shown in Figure 2. As mentioned earlier, fixed potential ($\phi = 0$) boundary condition is applied at the bottom wall. The top wall is treated by specifying average current density ($i = i_{applied}$).

Inflow boundary conditions with specified mass flow rate and species mole fractions are applied at both fuel and air channel inlets. The temperature of the air and fuel mixture entering at their respective channels is 1123 K. Also, both channels are operating at atmospheric pressure. Specified back pressure outflow conditions are applied at both air and fuel channel outlets.

Several transport processes take place at the anode-electrolyte and the cathode-electrolyte interfaces that strongly affect the overall behavior of the SOFC. The conversion of oxygen molecules into oxygen ions at the cathode-electrolyte interface is modeled by applying a mass flux condition at the interface using Faraday's law. In equation (13), i is the local current density and F is Faraday's constant. A negative sign implies that the flux is leaving the interface.

$$J_{O_2} = -\frac{i}{4F} M_{O_2} \tag{13}$$

Similarly, the following mass flux conditions for hydrogen and steam are applied at the anode-electrolyte interface.

$$J_{H_2} = -\frac{i}{2F} M_{H_2} \tag{14}$$

$$J_{H_2O} = \frac{i}{2F} M_{H_2O} \tag{15}$$

In order to account for the heat generated due to electrochemistry, heat flux proportional to the entropy change associated with the electrochemical reaction is applied at the anode-electrolyte and cathode-electrolyte interfaces. This heat flux is proportional to the molar formation rate, " $\frac{i}{n_e F}$ ", where n_e is the number of electrons participating in the electrochemical reaction.

2.3 Solution Procedure

Flowfield variables are computed using an unstructured, implicit, finite-volume solver. The solver is vertex centered and the discrete residual at each node is computed by integrating the governing equations, (1) – (6) over a median dual control volume. Because a steady-state solution is the primary goal of the current work, time accuracy of the solution is sacrificed by allowing local time-stepping to accelerate convergence.

To reduce computer time, the solution is obtained using multiple processors utilizing the message passing interface (MPI) [35] and necessary grid decomposition is achieved using METIS [36]. Original grids are generated using the commercial software Gridgen [37].

An implicit Euler scheme is used to solve the non-linear system as given by equations (1) - (6). A flux-difference splitting scheme based on the ROE scheme [38,39] for a multi-component mixture is derived to model the convective fluxes. A central-difference formulation is used to compute all the second-order derivative terms. Linear systems encountered in both the flowfield and sensitivity solvers are solved using the GMRES [40] method.

3. Design and Sensitivity Analysis

3.1 Discrete Adjoint Method

The goal of an adjoint method is to determine sensitivity derivatives that can be used in a formal optimization procedure for minimizing a specified cost function, which is indicative of the performance of the system. A general optimization procedure begins by first defining a meaningful cost function and a desired set of design variables. A numerical analysis of the baseline system is then performed. The results of the analysis include the solution variables Q of the discretized partial differential equations, which are subsequently used to determine the initial cost. Because the numerical analysis involves discretization of the partial differential equations on a computational mesh, it should be noted that Q represents the vector of solution variables where each element of the vector is representative of one or more physical variables located at each mesh point, χ.

The cost function may have an explicit dependence on the vector of design variables, β, but will also have an implicit dependence because Q and χ may also depend

on the design variables. Therefore, the cost function is typically written to indicate the implicit and explicit dependence on the design variables as,

$$f = f(Q(\beta), \chi(\beta), \beta) \tag{16}$$

If R represents the vector of discrete residuals at each mesh point, an augmented cost function L can be defined in the terms of the original cost function and the vector of discrete residuals as following.

$$L(Q(\beta), \chi(\beta), \beta, \Lambda) = f(Q(\beta), \chi(\beta), \beta) + \Lambda^T R(Q(\beta), \chi(\beta), \beta) \tag{17}$$

In equation (17), Λ is the vector of Lagrange multipliers (also known as costate variables). Note that the augmented cost function, L, is a scalar quantity that is identical to the original cost function f, when $R(Q)$ is zero, indicating that the steady-state solution is obtained. Differentiating the augmented cost function with respect to each of the design variables yields the following set of equations for $\frac{dL}{d\beta}$, which is a column vector where each element represents the derivative of the augmented cost function with respect to a particular design variable.

$$\frac{dL}{d\beta} = \left\{ \frac{\partial f}{\partial \beta} + \left[\frac{\partial \chi}{\partial \beta} \right]^T \frac{\partial f}{\partial \chi} \right\} + \left[\frac{\partial Q}{\partial \beta} \right]^T \left\{ \frac{\partial f}{\partial Q} + \left[\frac{\partial R}{\partial Q} \right]^T \Lambda \right\} + \left\{ \left[\frac{\partial R}{\partial \beta} \right]^T + \left[\frac{\partial \chi}{\partial \beta} \right]^T \left[\frac{\partial R}{\partial \chi} \right]^T \right\} \Lambda \tag{18}$$

Because the elements of Λ are arbitrary, the second term, which involves the derivatives of the dependent variables with respect to the design variables, can be eliminated by solving a linear system of equations for the costate variables, also known as the adjoint equation.

$$\left[\frac{\partial R}{\partial Q}\right]^T \Lambda = -\left\{\frac{\partial f}{\partial Q}\right\} \tag{19}$$

Once the costate variables are obtained, the derivatives of the cost function with respect to all the design variables are obtained using a matrix-vector multiplication.

$$\frac{\mathrm{d}L}{d\beta} = \left\{\frac{\partial f}{\partial \beta} + \left[\frac{\partial \chi}{\partial \beta}\right]^T \frac{\partial f}{\partial \chi}\right\} + \left\{\left[\frac{\partial R}{\partial \beta}\right]^T + \left[\frac{\partial \chi}{\partial \beta}\right]^T \left[\frac{\partial R}{\partial \chi}\right]^T\right\} \Lambda \tag{20}$$

In numerical simulations, the largest computational cost of computing sensitivity derivatives using the adjoint equations is due to the solution of the analysis equations and the adjoint equation, both of which are independent of the number of design variables. The only dependency on the number of design variables is in the evaluation of equation (20), which is generally much cheaper to compute than either the analysis or adjoint solutions.

Note that the terms in equations (18) - (20) involve differentiation of the discrete residual R, the cost function f, and the computational mesh χ with respect to the dependent variables Q, the design variables β, and the location of the mesh points χ. Correct implementation of this procedure can be extremely tedious to accomplish by hand and the resulting code can be difficult to maintain. To overcome the difficulties associated with hand differentiation, the complex-variable technique of Burdyshaw et al. [18] and Nielsen et al. [26] has been used for evaluating all the terms in the matrices required for solving the adjoint equations and for evaluating equation (20) once the costate variables have been obtained. Step-by-step derivation of complex variable technique is demonstrated by Kapadia et al. [28] along with the detailed discussion on relative benefits

and drawbacks of complex variable method with respect to automatic differentiation [41,42] and finite difference methods.

3.2 Mesh Sensitivity

As described earlier, the optimization procedure presented using the three-dimensional SOFC model in this work allows shape parameters as design variables. To maintain the quality of the mesh during a design cycle, a methodology is required to compute the displacements of the interior nodes when the underlying geometry is modified. The present simulations use the linear elasticity equations as applied in reference [43] to compute these displacements as shown in equation (21).

$$[\Gamma]\chi = \chi_{surface} \tag{21}$$

The matrix, $[\Gamma]$, is formed by applying a finite-volume method to the linear elasticity equations and $\chi_{surface}$ denotes the displacements applied to the surface nodes. Note that, $[\Gamma]$ does not depend on the vector of the design variables, β. Thus, by differentiating equation (21) with respect to β, mesh sensitivities, $\partial\chi/\partial\beta$ can be obtained.

$$[\Gamma]\frac{\partial\chi}{\partial\beta} = \frac{\partial\chi_{surface}}{\partial\beta} \tag{22}$$

Using equation (22), sensitivities are computed separately for each shape parameter and are then used in equation (20) for determining the sensitivity derivatives. Because this procedure is repeated for each design variable, it can be computationally prohibitive for

three-dimensional design problems when many parameters are present. To overcome this difficulty, the method developed by Nielsen and Park [44] has been implemented in the current study. In this technique, satisfaction of the mesh equation given by equation (21) is included as a further constraint in the augmented cost function.

$$L(Q(\beta),\chi(\beta),\beta,\Lambda) = f(Q(\beta),\chi(\beta),\beta) + \Lambda^T R(Q(\beta),\chi(\beta),\beta) + \Lambda_g^T\left([\Gamma]\chi - \chi_{surface}\right) \tag{23}$$

Here, Λ_g is the vector of co-state variables associated with the mesh displacements. The last term in equation (23) represents the residual of the linear system presented in equation (21), which is zero when the solution is converged. Thus, equation (23) maintains the original value of the desired cost function, f. Equation (24) is obtained by following the same procedure used in deriving equation (20).

$$\frac{dL}{d\beta} = \frac{\partial f}{\partial \beta} + \left[\frac{\partial R}{\partial \beta}\right]^T \Lambda + \left[\frac{\partial Q}{\partial \beta}\right]^T \left\{\frac{\partial f}{\partial Q} + \left[\frac{\partial R}{\partial Q}\right]^T \Lambda\right\} + \left[\frac{\partial \chi}{\partial \beta}\right]^T \left\{\frac{\partial f}{\partial \chi} + \left[\frac{\partial R}{\partial \chi}\right]^T \Lambda + [\Gamma]^T \Lambda_g\right\} - \Lambda_g^T \left[\frac{\partial \chi_{surface}}{\partial \beta}\right] \tag{24}$$

Finally, the grid adjoint problem, equation (25), is derived by solving for Λ_g to eliminate the mesh sensitivity term, $(\partial\chi/\partial\beta)^T$ in a similar manner as the first adjoint problem.

$$[\Gamma]^T \Lambda_g = -\frac{\partial f}{\partial \chi} - \left[\frac{\partial R}{\partial \chi}\right]^T \Lambda \tag{25}$$

Note that with this procedure, Λ is first obtained and subsequently used on the right-hand side of equation (25). Although equation (25) represents an additional linear system of equations, the effects of mesh sensitivities for each design variable are accounted for in a programming loop extending only over surface coordinates and eliminates the need for multiple solutions of equation (21). By combining equations (19), (24) and (25), sensitivity derivatives of an augmented cost function can be computed using equation (26).

$$\frac{dL}{d\beta} = \frac{\partial f}{\partial \beta} + \left[\frac{\partial R}{\partial \beta}\right]^T \Lambda - \Lambda_g^T \left[\frac{\partial \chi_{surface}}{\partial \beta}\right] \tag{26}$$

3.3 Parameterization

Recently, a parameterization method has been developed to improve the flexibility and speed in which a shape design problem can be defined. This method uses a construct called a control grid [45], which is associated with the surface mesh upon which shape modification is desired. Design variables are defined on the boundaries of the control grid as perturbation sources, which are then propagated to the surface mesh. In this case, the perturbations are propagated via an elliptic PDE solve (Laplacian) over the control grid volume. The resulting surface displacements are linear functions of the design variables. As a consequence, the parameterization need only be computed for the original surface mesh. Subsequent shape deformations are then computed as a linear combination of the design variable values and their associated sensitivity derivatives which are also computed only for original surface. This tool has been used to define a parameterization for a wide variety of shapes, including turbomachinery blades, wing/spar combinations, and an inlet

s-duct. In Case 1, the parameterization technique has been used to provide design variables to control the width of the 17 channels, while treating the baffles as rigid bodies. In Case 2, design variables are located on the top and bottom walls of the fuel channel as shown in Figure 3.

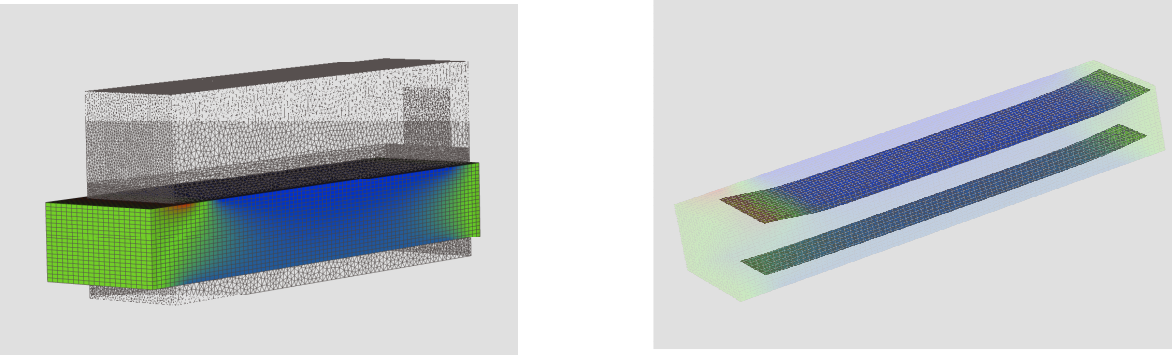

Figure 3. Parameterization applied in Case 2

3.4 Optimization

The optimization method used in this case is the quasi-Newton method of Broyden, Fletcher, Goldfarb, and Shanno (BFGS) combined with a Trust Region method for the step size. Side constraints are enforced in the step size calculation where those variables at the bounds are excluded from the step calculation.

As previously mentioned, mesh movement was accomplished by modeling the mesh as a linearly elastic medium in which stresses are caused the rigid body motion of the surfaces. The forces due to these stresses are then balanced by solving the linear elasticity equations on the mesh, which prescribe a redistribution of the interior mesh points.

4. Results and Discussion

Case 1

Figure 1(b) shows the computational model utilized in Case 1, which is loosely based on an experimental geometry from the University of Arizona as shown in Figure 1(a). Incompressible, viscous (laminar) flow solver has been utilized to calculate the flowfield variables.

As seen in Figure 4(a), the original flow field has a significant amount of uneven flow distribution through the channels such that most of the fluid moves through the first four, and last three channels, and is relatively stagnant in the remaining ten. This design is clearly inefficient with respect to fuel utilization, which becomes a critical issue as current draw is increased.

To obtain better fuel distribution throughout the cell, an infinite variety of surface modifications may be investigated. However, for these results, the widths of the channels are allowed to vary, so that the final design would likely be easily manufactured. Figure 4(b) shows the improved design shaded with x-coordinate velocity contours.

The design optimization was performed, in which the objective was to minimize the standard deviation of the flow velocity through the midpoint of each channel from the average velocity of all the channels. The resulting design depicted in Figure 4(b) produced an 80% reduction in the cost function compared with the original. Comparison of average velocity inside each channel between the original geometry and the optimized geometry is shown in Figure 5 and demonstrates that significant improvement in the distribution of the flow has been achieved.

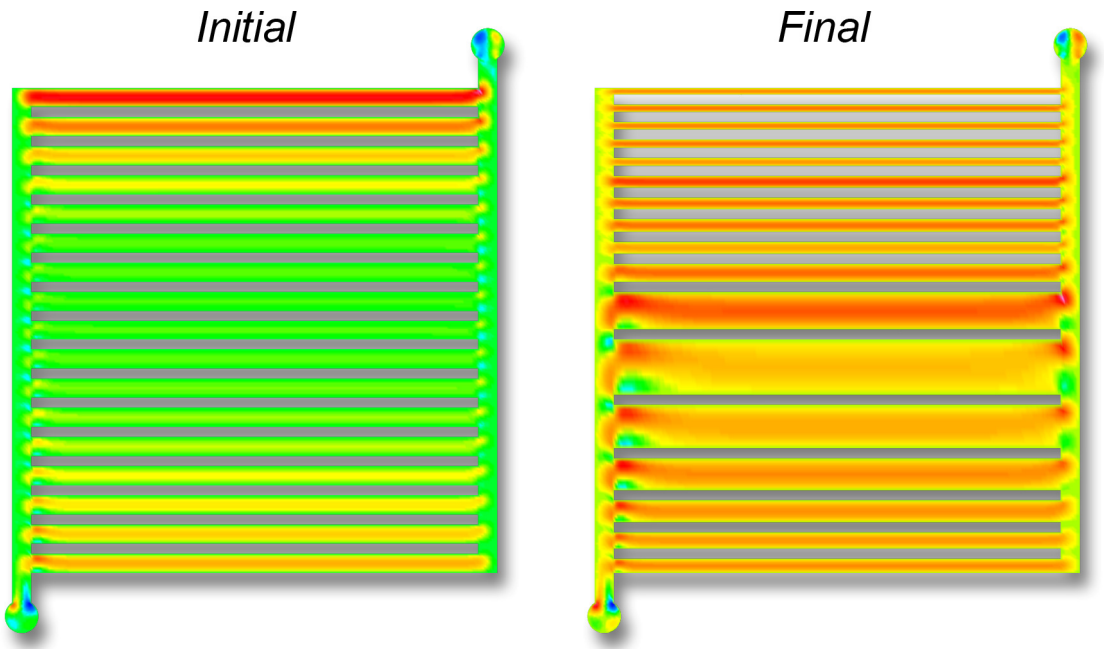

Figure 4(a) & (b). Initial and improved manifold geometries

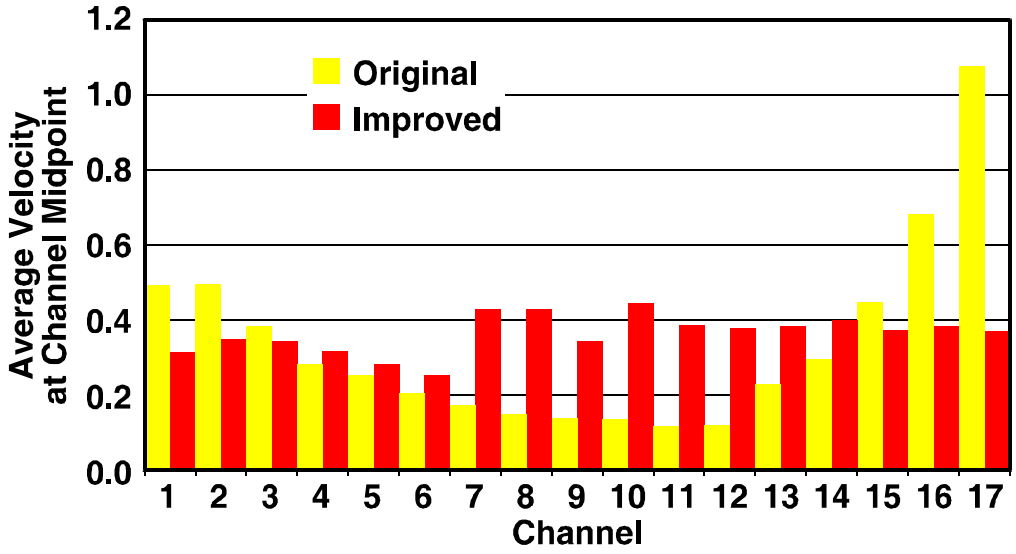

Figure 5. Average velocity in each channel of baseline and improved manifold designs

Case 2

The operating conditions utilized in the simulation are described in Table 5. As

seen in Table 5, partially reformed fuel has been utilized and thus, two chemical reactions, water gas shift (27.1) and methane reforming (27.2) reactions have been considered inside the anode.

X_{CO}	X_{H_2O}	X_{CO_2}	X_{H_2}	X_{CH_4}	X_{O_2}	X_{N_2}	$T(K)$	$P(N\ m_2)$
0.029	0.493	0.044	0.263	0.171	0.198	0.802	1123 K	101325
Table 5. Mole fractions and operating conditions								

$$CH_4 + H_2O \underset{kb_r}{\overset{kf_r}{\rightleftharpoons}} CO + 3H_2 \tag{27.1}$$

$$CO + H_2O \underset{kb_s}{\overset{kf_s}{\rightleftharpoons}} CO_2 + H_2 \tag{27.2}$$

Reaction rates for various species have been computed using the following equations.

$$Rate_r = kf_r\, p_{CH4}\, p_{H2O} - kb_r\, p_{CO}\, p_{H2}^3 \tag{28.1}$$

$$Rate_s = kf_s\, p_{CO}\, p_{H2O} - kb_s\, p_{CO2}\, p_{H2} \tag{28.2}$$

Subscripts "r" and "s" stand for reforming and shift reactions, respectively. Reaction rate constants, kf and kb, are computed using the methodology outlined in reference [29]. Mass flow rates of fuel and air are 3.0 x 10^{-7} kg/sec and 1.76 x 10^{-5} kg/sec, respectively. Current density of 8000 A/m^2 is applied at the top wall of the computational geometry shown in Figure 2.

Improving power output is the ultimate goal of the SOFC design. If current density is fixed, the power output can be improved by increasing the cell voltage. Sensitivity derivatives of the cost function representing the cell voltage with respect to various design

parameters can be extremely useful in the design cycle. Thus, the following cost function is considered for sensitivity analysis and optimization.

$$f = \frac{1}{S_t} \iint_{S_t} \phi \, ds \quad S_t - \text{Surface area of the top surface} \tag{29}$$

Eighteen design parameters are utilized in the design cycle. Design parameters are located on the top and bottom surfaces of the fuel channel. Only normal movements of both surfaces are allowed. Design parameters are defined in a manner such that the inlet plane of the fuel channel stays fixed while allowing for movement of the outlet plane. Though not attempted in the present study, optimization of material properties and operating conditions can also be integrated with the shape optimization with ease [29].

As mentioned earlier, the top and bottom surfaces of the fuel channel are allowed to move during the optimization cycle. The top surface of the fuel channel is also shared by the anode as shown in Figure 2 and thus, the anode shape may be modified during optimization. Figure 6 shows the original and modified anode shape obtained during optimization. As seen, the average thickness of the anode has been increased during design. An explanation of this result can be obtained by considering that the reforming and shift reactions, given by equations (27.1) and (27.2), are responsible for the generation of hydrogen. As chemical reactions are only allowed to take place inside the anode, a thicker anode provides increased volumetric generation rate of hydrogen, which is not negated by increased ohmic losses. As electrochemical reactions are responsible for the consumption of hydrogen, additional hydrogen generated due to the increased volume of the anode also assists in lowering concentration polarization. An interesting feature of the

optimized anode in Figure 6 is that the thickness of both ends remain approximately same even though movement of one end located above the outlet plane has not been restricted.

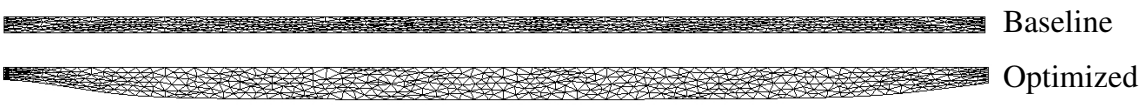

Figure 6. Shape of the anode before and after optimization

Figure 7 shows hydrogen mole fractions contours plotted at four streamwise locations for both baseline and optimized geometries. Reduction in hydrogen mole fraction is evident as fuel moves from the inlet towards the outlet of the channel in both geometries. Also, the corner indicated by "Point-A" represents the location containing the lowest hydrogen mole fraction in both cases. As seen, "Point–A" is located at the anode-electrolyte interface, directly above the interconnect. The "Point-A" in Figure 7 is not in direct contact with the fuel channel and thus, fresh hydrogen from the channel has to travel over an extended diffusion path to provide sufficient hydrogen required by the electrochemical reactions taking place at the anode-electrolyte interface. As mentioned earlier, reforming and shift reactions act as local sources of hydrogen inside the anode. By closely comparing the first three planes for both the baseline and optimized geometries in Figure 7, one can observe the effect of the thicker anode in providing more hydrogen at the corner indicated by "Point-A". This effect ultimately transforms into the reduction of concentration polarization at the anode-electrolyte interface and thus, increases the cell voltage.

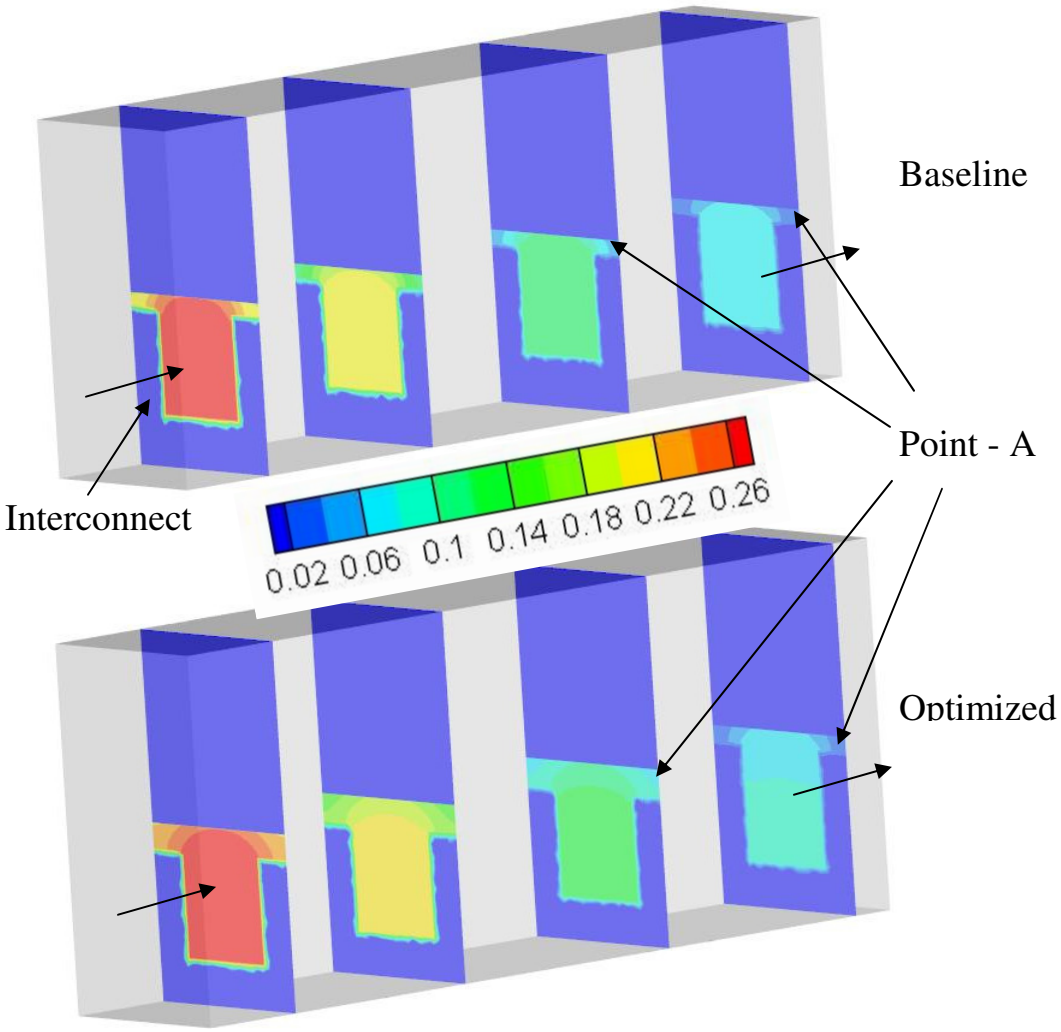

Figure 7. Hydrogen mole fraction at different streamwise locations

This case represents a single-point optimization, where a current density of 8000 A/m^2 has been applied in design study to optimize the shape of the fuel channel and the anode as shown in Figure 7. Using the new geometry, a series of test cases with different current densities and same inlet species concentrations given in Table 5 have been run to check the generality of the improvement achieved. The comparison between the polarization curves obtained using the baseline and optimized geometries is shown in Figure 8. As expected, the cell voltage reduces with increasing current density for both

geometries due to the combined effects of ohmic polarization and concentration polarization. The steepest reduction in cell voltage can be observed between current densities of 7500 A/m^2 and 8000 A/m^2. Also, the optimized geometry consistently demonstrates better performance than baseline geometries for all current densities. However, because the optimization cycle has been done at a single operating condition, this can not be expected to represent a general result. Multipoint optimization methodologies are needed and are currently under development.

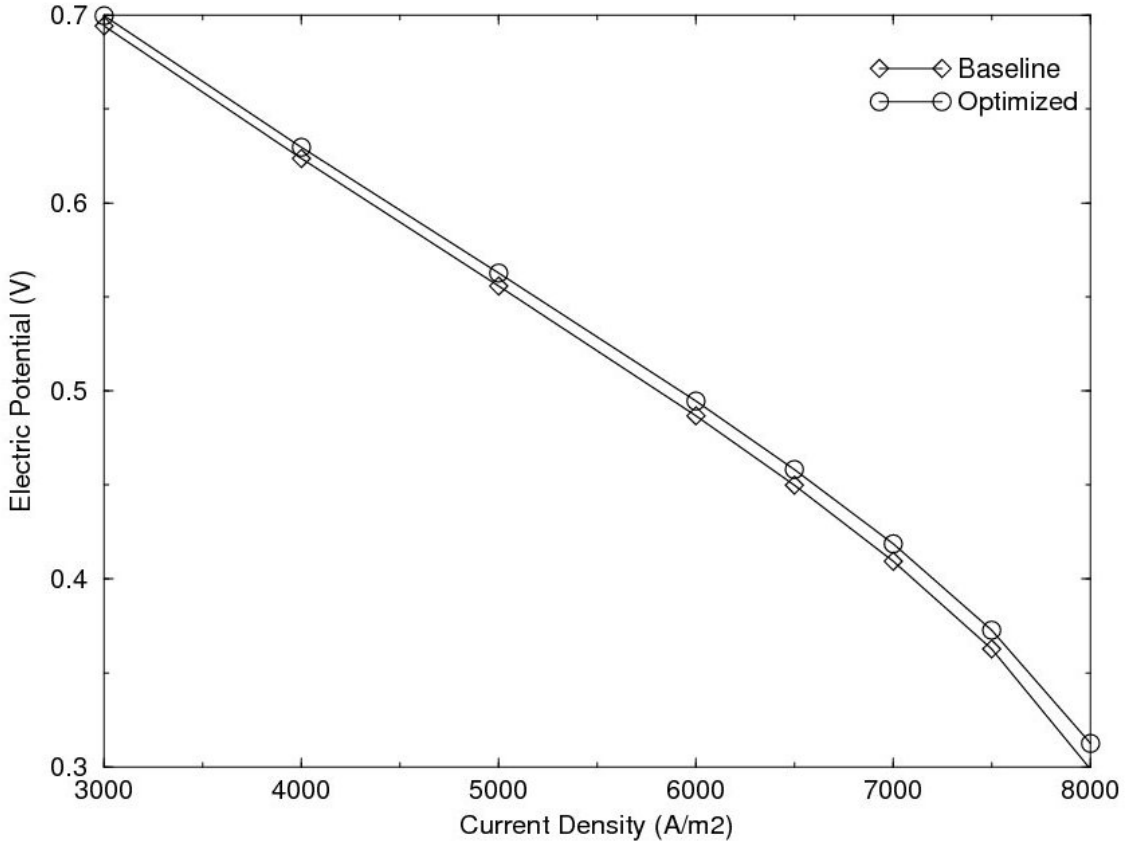

Figure 8. Comparison of polarization curve between baseline and optimized geometry

Even though Figure 8 shows better results with the optimized geometry, it is hard to quantify the improvements achieved at each current density. Thus, quantitative

improvement in the cost function is shown in Figure 9. As expected, the percentage improvement in cell voltage increases with the increase in the current density. The reason behind such behavior is that the consumption rate of the hydrogen at the anode-electrolyte interface is directly proportional to the current density as shown in equation (14). Therefore, the effect of the additional hydrogen resulting from the thicker anode is more evident for cases with higher current densities. In Figure 9, improvement in cost function is almost linear (0.8% – 2.25 %) for current densities ranging from 3000 – 7000 A/m^2, but increases rapidly from 2.25% to 4.6% as current density is increased from 7000 A/m^2 to 8000 A/m^2.

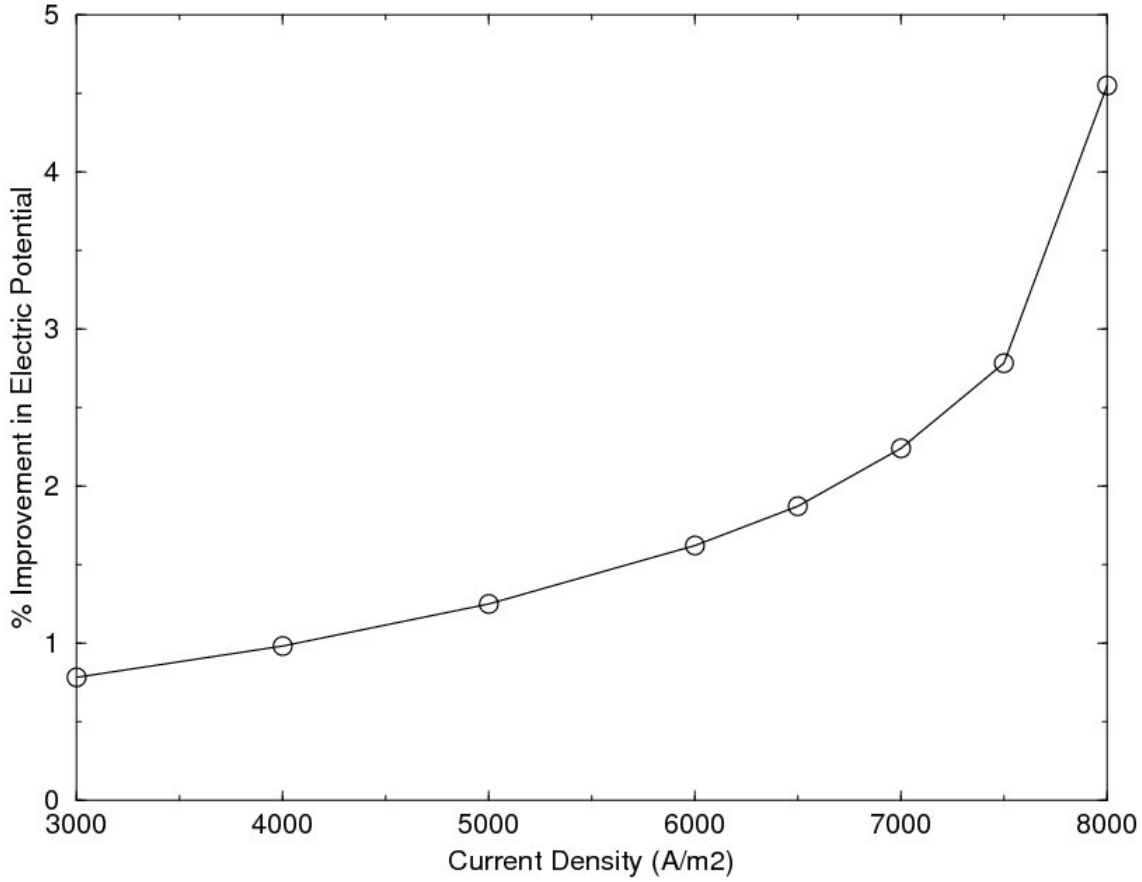

Figure 9. Quantitative analysis of cost function improvement

5. Conclusions and Future Work

An automated design tool has been developed to perform shape optimization of SOFC components. Various processes involving flowfield solution, sensitivity computation, geometric parameterization, mesh movement and optimization have been integrated under a single frame work. A three-dimensional, parallel, unstructured solver has been developed to model complicated transport phenomena present inside all components (channels, electrodes, electrolyte and interconnects) of a solid oxide fuel cell. Two different geometries have been utilized in optimization procedure. In the first problem, a manifold containing seventeen channels has been modified to obtain uniform distribution of fuel among all channels. Here, the channel width is allowed to change to improve the cost function. In the second problem, optimization of a single channel SOFC has been attempted to achieve higher cell voltage. Average thickness of the anode has been increased in the optimized geometry of a single-channel SOFC. Polarization curve comparison between the baseline and the optimized geometry demonstrates that the modified geometry can achieve improved results, particularly cases running at high current densities.

Future work is targeted at developing multipoint optimization capability and for extending the present work for polymer electrolyte membrane (PEM) fuel cells. Also, time-dependent simulations will be implemented to study the transient behavior of the SOFC.

Acknowledgements

This work was supported by the Office of Naval Research grant number N00014-08-1-0217, 5kW Planar Solid Oxide Fuel Cell Demonstration and Simulations Research for Analysis and Design of SOFC's and the Tennessee Higher Education Commission (THEC) Center of Excellence in Applied Computational Science and Engineering. This support is greatly appreciated.

Nomenclature

Symbols		**Unit**
B	Permeability	m2
E_t	Total energy	J/m3
f	Cost function	cost function depended
H	Enthalpy	J kg_1
i	Current density	A m_2
i_0	Exchange current density	A m_2
J	Mass flux vector	kg m_2s_1
L	Augmented cost function	cost function dependent
$\dot{m}$	Mass flow rate	kg s_1
M	Molecular weight	kg kmol_1
ns	Number of species	-
P	Pressure	N m_2
Q	Solution vector	solution variable dependent

q	Heat flux	J m_2 s_1
T	Temperature	K
u	x-velocity component	m s_1
v	y-velocity component	m s_1
w	z-velocity component	m s_1
x,y,z	Co-ordinate system	-
X_i	Mole fraction of i th species	-
Y_i	Mass fraction of i th species	-

Greek Symbols

β	Design variable vector	design variable dependent
χ	Grid vector	m
ρ	Mass concentration	kg m_3
μ	Molecular viscosity	kg m s_1
ϕ	Electric potential	volt
η	Activation polarization	volt
Λ	Costate variable vector	cost function dependent
ε	Porosity	-
κ	Totruosity	-
$\forall$	Control volume	m3
τ	Viscous flux	kg m_1 s_2

Constants

F	Faraday constant	96484.56	A- s mol_1
R_u	Universal gas Constant	8314.4	J kmol_1 K_1

Indices

a	Anode
c	Cathode
eff	Effective
i, j	Chemical species

References

[1] Ferguson, J. R., Fiard, J. M., Herbin, R., “Three-Dimensional Numerical Simulations for Various Geometries of Solid Oxide Fuel Cells”, J. Power Sources, 58 (1996) 109-122.

[2] Fiard, J. M., Herbin, R., “Comparison Between Finite Volume and Finite Element Methods for an Elliptic System Arising in Electrochemical Engineering”, Comp. Methods in App. Mech. and Eng., 115, (1994) 315-338.

[3] Haberman, B. A., Young, J. B., “Three-Dimensional Simulation of Chemically Reacting Gas Flows in the Porous Support Structure of an Integrated-Planar Solid Oxide Fuel Cell”, Int. J. of Heat and Mass Transfer, 47, (2004) 3617-3629.

[4] Khaleel, M. A., Lin, Z., Singh, P., Surdoval, W., Collin, D., "A finite element analysis modeling tool for solid oxide fuel cell development: coupled electrochemistry, thermal and flow analysis in MARC", J. of Power Sources, 130, (2004) 136-148.

[5] Lehnert W., Meusinger J., Thom F., "Modelling of gas transport phenomena in SOFC anodes", J. Power Sources, 87, (2000) 57-63.

[6] Li P. W., Chyu. M. K., "Simulation of the Chemical/Electrochemical Reaction and Heat/Mass Transfer for a Tubular SOFC Working in a Stack", J. Power Sources, 124, (2003) 487-498.

[7] Chan, S. H., Khor, K. A., Xia, Z. T., "A complete polarization model of a solid oxide fuel cell and its sensitivity to the change of cell component thickness", J. Power Sources, 93, (2001) 130-140.

[8] Campanari, S., Iora, P., J. Power Sources, "Definition and sensitivity analysis of a finite volume SOFC model for a tubular cell geometry", 132 (2004) 113-126.

[9] Grujicic, M., Chittajallu, K. M., "Design and optimization of polymer electrolyte membrane (PEM) fuel cells", Applied Surface Sci., 227 (2004) 56-72.

[10] Grujicic, M., and Chittajallu, K. M., "Optimization of the cathode geometry in polymer electrolyte membrane (PEM) fuel cells", Chem. Eng. Sci., 59 (2004) 5883-5895.

[11] Anderson, W.K., Newman, J.C., Whitfield, D.L., Eric Nielsen, E.J., "Sensitivity Analysis for the Navier-Stokes Equations on Unstructured Meshes Using Complex Variables", AIAA Journal, 39, 1, (2001) 56-63.

[12] Burden, R. L., Faires, D. J., "Numerical Analysis", Sixth Edition, Brooks/Cole Publishing Company, 1997, 16-26.

[13] Secanell, M., Djilali, N., Suleman, A., “Optimization of a planar self-breathing PEM fuel cell cathode”, AIAA 2006-6917, 11th AIAA/ISSMO Multidisciplinary Analysis and Optimization Conference, 6-8 Sept., 2006, Portsmouth, Virginia.

[14] Huang, C. M., Shy, S. S., Lee, C. H., “On flow uniformity in various interconnects and its influence on cell performance of planar SOFC”, J. Power Sources, 183, (2008) 205-213.

[15] Lee, S., Jeong, H., Ahn, B., Lim, T., Son, Y., “Parametric study of the channel design at the bipolar plate in PEMFC performances”, I. J. of Hydrogen Energy, 33, (2008) 5691-5696.

[16] Anderson, W. K., Venkatakrishnan, V., “Aerodynamic Design Optimization on Unstructured Grids with a Continuous Adjoint Formulation”, Computers and Fluids, 28, 4-5, (1999) 443-480.

[17] Anderson, W. K., Bonhaus, D. L., “Airfoil Design on Unstructured Grids for Turbulent Flows”, AIAA Journal, 37, 2, (1999) 185-191.

[18] Burdyshaw, C. E., Anderson, W. K., “A General and Extensible Unstructured Mesh Adjoint Method”, AIAA J. of Aerospace, Computing, Information, and Communication, 2, 10, 401-413 (2005).

[19] Burdyshaw, C. E., “Achieving Automatic Concurrency Between Computational Field Solvers and Adjoint Sensitivity Codes,” Ph.D. Thesis, University of Tennessee, Chattanooga, May, 2006.

[20] Jameson, A., “Aerodynamic Design Via Control Theory”, J. Scientific Computing, 3, (1998) 233-260.

[21] Jameson, A., Alonso, J. J., Reuther, J., Martinelli, L., Vassberg, J. C., “Aerodynamic Shape Optimization Techniques Based on Control Theory”, AIAA Paper No. 98-2538, (1998).

[22] Mohammadi, B., “Optimal Shape Design, Reverse Mode of Automatic Differentiation and Turbulence”, AIAA Paper No. 97-0099, (1997).

[23] Nielsen, E. J., Anderson, W. K., “Recent Improvements in Aerodynamic Optimization on Unstructured Meshes”, AIAA J., 40, 6, (2002) 1155-1163.

[24] Nielsen, E. J., Anderson, W. K., “Aerodynamic Design Optimization On Unstructured Meshes Using the Navier-Stokes Equations”, AIAA J., 37, 11, (1999) 1411-1419.

[25] Nielsen, E. J., “Aerodynamic Design Sensitivities on an Unstructured Mesh Using the Navier-Stokes Equations and a Discrete Adjoint Formulation”, Ph.D. Dissertation, Virginia Polytechnic Institute and State University, (1998).

[26] Nielsen, E. J., Kleb, W. L., “Efficient Construction of Discrete Adjoint Operators on Unstructured Grids by Using Complex Variables”, AIAA J., 44, 4 (2005) 827-836.

[27] Park, M., “Adjoint-Based, Three-Dimensional Error Prediction and Grid Adaptation”, AIAA Paper No. 2002-3286, (2002).

[28] Kapadia S., Anderson W. K., Elliott L., Burdyshaw C., “Adjoint method for solid-oxide fuel cell simulations”, J. Power Sources, 166 (2007) 376-385.

[29] Kapadia S., Anderson W. K., Elliott L., Burdyshaw C., "Adjoint based Sensitivity Analysis and Error Correction Methods applied to Solid Oxide Fuel Cells", ASME J. Fuel Cell Sci. Tech., 6, 2, (2009).

[30] Kapadia S., Anderson W. K., "Sensitivity Analysis for Solid Oxide Fuel cells using a Three-Dimensional Numerical Mode", J. Power Sources, 189 (2009) 1074-1082.

[31] Wang, Y., Yoshiba, F., Watanbe, T., Weng, S., "Numerical analysis of electrochemical characteristics and heat/species transport for planar porous-electrode-supported SOFC", J. Power Sources, 170, (2007) 101-110.

[32] Hwang, J. J., Chen, C. K., Lai, D. Y., "Computational analysis of species transport and electrochemical characteristics of a MOLB-type SOFC", J. Power. Sources, 140, (2005) 235-242.

[33] Noren, D. A., Hoffman, M. A., "Clarifying the Butler-Volmer equation and related approximation for calculating activation losses in solid oxide fuel cell models", J. Power Sources, 152, (2005) 175-181.

[34] Costamagna, P., Selimovic, A., Borghi, M., Agnew, G., "Electrochemical model of the integrated planar solid oxide fuel cell (IP-SOFC)", Chem. Eng. J., 102, (2004) 61-69.

[35] Grama A., Gupta, A., Karypis, G., Kumar, V., "Introduction to Parallel Computing", Second Edition, Addison Wesley, Jan. 16, 2003.

[36] METIS webpage: http://glaros.dtc.umn.edu/gkhome/views/metis

[37] Gridgen webpage: http://www.pointwise.com/gridgen

[38] Roe, P. L., "Characteristic-based schemes for the Euler equations", Ann. Rev. Fluid Mech., 18, (1986) 337-365.

[39] Busby M., “Steps Toward More Accurate and Efficient Simulations of Reactive Flows”, Ph.D. Thesis, Mississippi State University, August 1997.

[40] Saad, Y., Schultz, M. H., “GMRES: A Generalized Minimal Residual Algorithm for Solving Nonsymmetric Linear Systems”, SIAM J. Sci. Stat. Comput., 7, (1986) 856-869.

[41] Bischof C., Roh L., Mauer-Oats A., “ADIC: an extensible automatic differentiation tool for ANSI-C”, Software: Practice and Experience, 27, 12, (1999), pp. 1427-1456.

[42] Cusdin P. A., “Automatic Sensitivity Code for Computational Fluid Dynamics”, Ph.D. Thesis, School of Aeronautical Engineering, Queen’s University, Belfast, U.K. (2005).

[43] Karman, S. L Jr., Anderson, W. K., Sahasrabudhe M.,”Mesh Generation Using Unstructured Computational Meshes and Elliptic Partial Differential Equation Smoothing”, AIAA J., 44, 6, June 2006.

[44] Nielsen, E. J., Park, M. A., “Using An Adjoint Approach to Eliminate Mesh Sensitivities in Computational Design”, AIAA J., 44, 5, (2006) 948-953.

[45] Anderson, W. K., Karman, S. L., Burdyshaw, C., "Geometry Parameterization Using Control Grids," Presented at the 12th AIAA/ISSMO Multidisciplinary Analysis, 2008.